Environmental Science
Water Research & Technology

Adsorption of Crude Oil from Crude Oil-Water Emulsion by Mesoporous Hafnium Oxide Ceramics

Journal:	*Environmental Science: Water Research & Technology*
Manuscript ID	EW-COM-05-2020-000451.R1
Article Type:	Communication

COMMUNICATION

Adsorption of Crude Oil from Crude Oil-Water Emulsion by Mesoporous Hafnium Oxide Ceramics

Received 00th January 20xx,
Accepted 00th January 20xx

DOI: 10.1039/x0xx00000x

Fatima A. Hussain,[a] Julio Zamora, [b] Ivonne M. Ferrer,[a] Maureen Kinyua[c] and Jesús M. Velázquez[a]*

We report a mesoporous hafnium oxide (MHO) ceramic synthesized via a sol-gel process that has exhibited 99.9% removal capacity of crude oil from an oil-in-water emulsion at a concentration of 3 mg/mL. The as-prepared MHO ceramic was regenerated after crude oil sequestration via calcination at 800°C under ambient conditions. The scalability of the synthetic method and thermal stability of the MHO ceramic material makes it a promising, underexplored, and reusable adsorbent for efficient oil spill clean-up.

Water Impact: Dispersants applied after an oil spill convert the oil on the surface to smaller droplets that travel deeper into the ocean, causing more damage to wildlife and marine ecosystems. This work brought to light mesoporous hafnium oxide (MHO) ceramics as a potential material for adsorption of crude oil. The MHO ceramics can be thermally regenerated after adsorption of emulsified crude oil, proving the reusability of the material as well. This underexplored adsorbent material can potentially minimize generated waste and associated cost of cleaning oil spills.

1 Introduction

Oil spills are a serious threat to marine life in an already vulnerable biosphere. For example, increased CO_2 emissions have caused elevated ocean temperatures, leading to coral reef bleaching and mortality.[1] Furthermore, local wildlife such as birds have also been adversely impacted by hypothermia as their feathers become covered in crude oil.[2] Humans can also be affected by oil spills through respiratory problems, skin irritation, and even cancer depending on the length and type of exposure.[3] Over 5 million tons of crude oil are transported annually by sea, and introduced to coastal waters that are extremely vulnerable to oil spills. Additionally, waste disposal, energy sources, accidents, and the production of oil are sources of water contamination. In 2010, the Deepwater horizon spill released 5 million barrels of oil worth 6 billion USD.[4] More recently, The Sanchi spill in 2018 in East China released ~1 million barrels of oil.[5]

As a response to oil spills, dispersants such as hydrophobically modified chitosan[6] and halloysite clay nanotubes[7] are sprayed over the spill area to prevent oil from spreading on the surface. These dispersants are composed of hydrophilic and lipophilic active sites and surround oil with the hydrophilic head facing outwards which helps stabilize the oil into small droplets. This allows for the oil droplets to move below the surface, making it seem like the surface is clean. However, this in turn leads to oil sedimentation in the ocean bed and negatively impacts aquatic life since the oil particles are not adsorbed by dispersants for subsequent removal.[8–11]

Adsorption is a preferred clean-up method because it is affordable, facile, and environmentally feasible.[12] There is a growing interest in the use of sorbent and reusable materials that are non-toxic to avoid further contamination of water. Some examples include agricultural waste (banana peels, palm fiber, rice husks),[12–14] polymeric materials coated on foams and sponges,[15–18] and aerogels made from carbon based materials such as cellulose[19] and graphene.[20] However, the lack of mechanical stability of these materials in harsh chemical environments limits their application.[21] Porous metal oxide ceramic materials such as silica, titania, hafnia, and zirconia are interesting candidates due to their relatively hydrophilic surfaces, which gives these materials particular advantages over hydrophobic ones. Their hydrophilic properties allow water to permeate, which prevents clogging by viscous and heavy oils. These materials also prevent the formation of a water layer under an oil layer as it will allow the water to permeate.[22–24]

[a] Department of Chemistry, University of California, One Shields Avenue, Davis, California 95616, USA.
[b] Material Science & Engineering, Washington State University, Pullman, Washington 99164, USA.
[c] Department of Civil & Environmental Engineering, University of California, One Shields Avenue, Davis, California 95616, USA.
† Footnotes relating to the title and/or authors should appear here.
Electronic Supplementary Information (ESI) available: [details of any supplementary information available should be included here]. See DOI: 10.1039/x0xx00000x

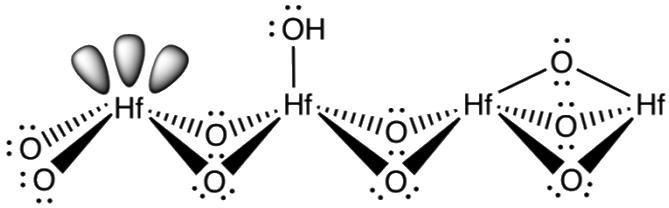

Fig. 1 Three main active sites on the surface of hafnium oxide: Lewis acid site (left), Brönsted acid site (middle), and Brönsted base site (right).

MHO monoliths with pores of different length scales are an attractive alternative to particles or pressed pellets, as they are thermally stable, mechanically robust, and allow for higher liquid mass transfer than powders.[25–28] The density of the MHO is slightly greater than that of water 1.1 g/cm^3. This characteristic, in addition to its hydrophilic nature, leads to strong enough interaction with water molecules to break surface tension and sink below the surface. This lack of buoyancy hinders the suitability for using MHO in batch adsorption experiments, although it is well suited for fixed-bed filtration experiments.

Hafnium oxide, a group IV transition metal oxide, is chemically and thermally stable due to the high coordination number of hafnium. Hafnium can coordinate to seven oxygen atoms, whereas silicon can only coordinate to four. This high degree of coordination makes hafnium oxide resistant to chemical degradation in extreme pH conditions, a highly desirable property for materials that will be exposed to harsh oil-removal conditions. Additionally, hafnium oxide contains three active sites on the surface: Brönsted base sites which accept a proton in basic media, Brönsted acid sites which donate a proton in acidic media, and Lewis acid sites originating from unoccupied hafnium d orbitals as shown in **Figure 1**. This broad network of bonding further contributes to the mechanical strength of hafnium oxide.[29]

The objective of this study is to investigate the efficiency of MHO for crude oil removal from crude oil-in-water emulsions. Sol-gel synthesis has been used for the synthesis of MHO to be integrated as a filter to sequester crude oil from crude oil-in-water emulsions in a wide pH range. Liquid aliquots have been analysed using chromatography and spectroscopy techniques. Regeneration of the MHO was studied through calcination and thermogravimetric analysis.

2 Experimental Section

2.1 Chemicals and Materials

Hafnium (IV) tetrachloride ($HfCl_4$, 98%), methanol, acetone, hexanes, and pentane were all HPLC Plus (>99.9%). Sulfuric acid (95.0-98.0%), hydrochloric acid (HCl, 35.0-37.0%), deuterated methanol (CD_3OD), and deuterated chloroform ($CDCl_3$) with tetramethylsilane (TMS) (99.95% + 0.05%) were used as purchased from Sigma-Aldrich. Poly(ethylene oxide) (MW 100,000) was purchased from Polysciences Inc. Propylene oxide (99.5%) was purchased from Acros Organics. N-methyl formamide (99%) and sodium hydroxide pellets (NaOH, 98%) were purchased from Alfa Aesar. Light crude oil (API > 31) was obtained from an un-disclosed oil refinery within northern California. Ultrapure water (resistivity >18.2 MΩ) used for synthesis and crude oil water mixes was obtained from a Thermo Scientific Barnstead E-Pure Ultrapure water purification system. Various porous materials were purchased for comparison purposes including melamine sponge (He Andi, pore size 150 μm), Whatman grade 1 cellulose filter paper (Sigma-Aldrich, pore size 11 μm), and a commercial wine filter (Buon Vino, no.2, pore size 1 μm).

2.2 Synthesis of MHO Ceramic Monolith

MHO ceramic monoliths were synthesized using the sol-gel method.[30] Prior to MHO synthesis, 20 mL scintillation glass vials were treated in sequence with 0.1 M NaOH for 1 hour, 0.1 M HCl for 1 hour, and Rain-x overnight. After removing the Rain-x, vials were rinsed with methanol three times and dried in an oven. Herein, we use hafnium (IV) chloride dissolved in ultrapure water in the hydrolysis step. N-methylformamide (NMF) was added as a porogen, to increase the solution pH, and induce phase separation. Polyethylene oxide (PEO, MW 100,000) was added to create a strong pore network. Additionally, propylene oxide was added to induce polymerization, turning the clear liquid to a white gel. The gel was then aged at 50°C for three days in air. The monolith was washed with ultrapure water, methanol, acetone, hexanes, and pentane to remove any excess reagents left after synthesis. Lastly, the sample underwent heat treatment in air to 700°C which yields a crystalline white monolithic ceramic.[30] The melamine sponge, cellulose filter paper, and a commercial wine filter with the same pore size as MHO were used for comparison. All materials were tested by vacuum filtration of a crude oil-in-water emulsion.

2.3 Structural Characterization of MHO Ceramic

After the synthesis, the crystalline structure and phase purity of the material was determined by powder X-ray Diffraction (XRD) using a Bruker D8 Advance diffractometer with Cu Kα radiation (1.5406 Å). Experimentally obtained diffraction patterns were then compared to literature patterns from the Inorganic Crystal Structure Database (ICSD) to confirm the structure. The mesostructure of the material was determined by a Thermofisher Quattro Environmental scanning electron microscope (ESEM). The sample was placed on copper tape and operated at an accelerating voltage of 10 keV under low vacuum. The surface of the MHO ceramic was analysed before filtration, after filtration, and after heating to remove crude oil (800°C) using Fourier Transform Infrared (FTIR) Spectroscopy. The Bruker Tensor 27 FTIR was equipped with an attenuated total reflectance (ATR) pike accessory. The experiment was performed using 16 scans, a resolution of 2 cm^{-1}, and a spectral range of 400 - 4000 cm^{-1}. Thermogravimetric Analysis (TGA) was done using a NETSCH STA 449F3 instrument under high purity argon. It was heated from 20°C to 800°C at a rate of 3.0 °C/min.

2.4 Oil Sequestration and MHO Ceramic Regeneration

In a typical oil sequestration experiment, crude oil was mixed with ultrapure water in a vial via sonication (Branson 8800, 40 kHz, ambient conditions) for 30 minutes to prepare the oil-in-water emulsion (2-3 mg/mL, pH 1, 7, and 13).[31] Sodium hydroxide and sulfuric acid were added to adjust the pH of the solution before adding the crude oil. The MHO ceramic monolith (0.2 - 0.4 g) was placed directly under the tip of a funnel using a shrinking tube as shown in **Fig S1a**. The funnel was then placed in a vacuum filtration setup as shown in **Fig S1b**. As previously mentioned, the hydrophilic nature of MHO as well as its bimodal pore network made it an ideal candidate for filtration of crude oil-in-water emulsions, rather than for adsorption in a batch-type system. The crude oil-in-water emulsion was analysed before and after filtration for comparison. The filtration procedure was repeated with various porous materials such as melamine sponge, grade 1 cellulose filter paper, and commercial wine filter. The MHO ceramic was regenerated after filtration by calcination in air at 800°C for 10 mins.

2.5 Qualitative and Quantitative Analysis of Oil Sequestration

The crude oil-in-water emulsion was analysed for crude oil concentration before and after filtration using an Agilent 6890 gas chromatograph equipped with a single quadrupole 5973 mass selective detector. In order to prepare samples suitable for GC-MS the liquids were extracted in pentane. A liquid-liquid extraction was done using 5 mL of the crude oil-in-water emulsion before or after filtration with 2 mL of pentane. The sample was placed in a glass centrifuge tube and centrifuged at 4500 rpm for 30 minutes. The pentane layer was injected in the GC. Compounds were separated on a Chrompack CP5860 (30 m, 0.25 mm ID, 0.25 um). The chromatograph oven was operated from 40°C to 300°C rising at a rate of 10 °C/min. Helium was used as the carrier gas operating at a pressure of 6.7 psi. An injection volume of 1 μL was used and the injection temperature was 300°C.[32] The mass spectrometer source temperature was 230°C and the quadrupole temperature was set to 180°C. The range of ionization was from 50.00 amu to 800.00 amu. The GC provides a qualitative approach to assess removal efficiencies. Nuclear magnetic resonance (NMR) spectroscopy was used for quantitation. ^{1}H NMR spectroscopy was performed on a Bruker 400 MHz spectrometer. Calibrations were performed with various concentrations of crude oil-in-water emulsions. 100 μL of the emulsion was added to 695 μL of deuterated methanol and 5 μL of $CDCl_3$ with TMS as an internal standard and mixed well. 400 μL of this matrix is placed in a 300 MHz Wilmad NMR tube for analysis. A presaturation method was used to suppress the signal of water and to allow visualization of the analyte peaks of interest. The area under the crude oil peaks is used to create a calibration to quantitatively determine the amount of oil removed by the material. To calculate the percent removal of crude oil we use the following equation:

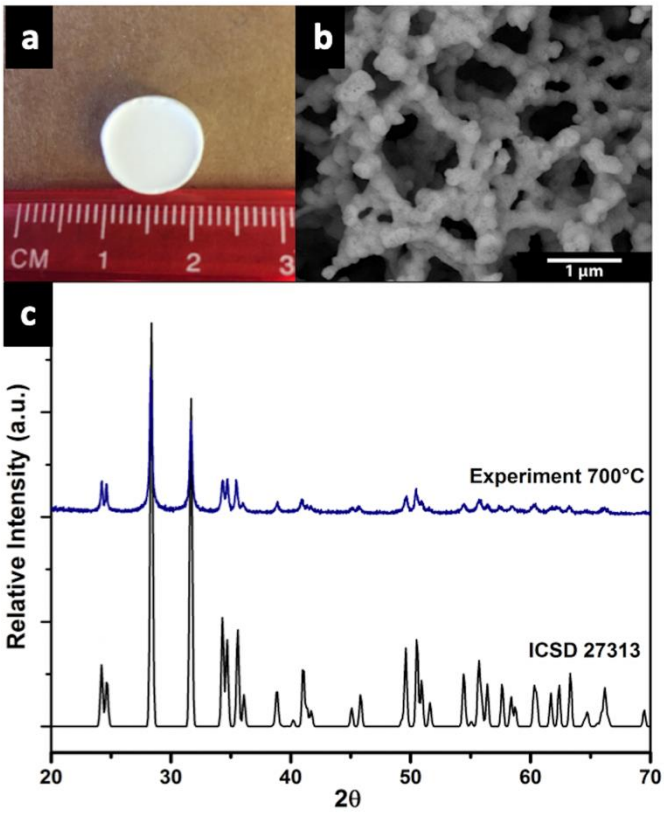

Fig. 2 a) Free standing MHO ceramic with a diameter of 1 cm, b) SEM image of MHO ceramic illustrating network of macropores and mesopores, c) XRD pattern with major diffraction peaks indexed for MHO ceramic (top) overlaid with the published spectrum for MHO with heat treatment at 700°C (bottom, ICSD Collection Code 27313).

$$\% \, Removal = \frac{C_0 - C}{C_0} \times 100$$

Where C_0 is the initial concentration of crude oil in water before filtration (mg/mL) and C is the concentration of crude oil in the filtrate.

3 Results and Discussion

3.1 Crystal Structure and Morphology of MHO Ceramic Monolith

The MHO ceramic monolith obtained after synthesis is shown in **Figure 2a**. The size and shape depend on the gelation vessel, which in this case was a 20 mL scintillation glass vial. **Figure 2b** depicts the MHO ceramic bimodal distribution comprised of a network of macropores and mesopores. The macropores are interconnected and appear to be approximately 1.0 μm in diameter based on the SEM. The monoclinic crystalline structure was confirmed by XRD and compared to literature values as shown in **Figure 2c**.

3.2 Determination of Oil Concentrations Sequestered

To determine the potential of MHO ceramics to sequester oil mixtures of 2-3 mg/mL of crude oil in water were prepared. These concentrations are relevant but slightly higher than

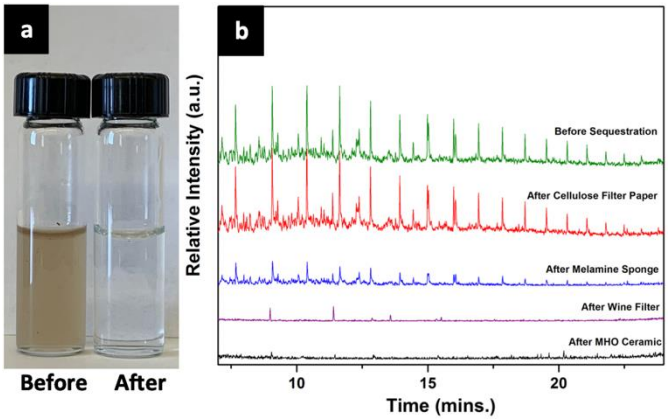

Fig. 3 a) Image of crude oil-in-water emulsion in vials before and after filtration via MHO ceramic monolith in neutral pH, b) Overlay GC-MS chromatograms of crude oil-in-water emulsion before sequestration and recovered liquid after sequestration using grade 1 cellulose filter paper, melamine sponge, commercial wine filter, and MHO ceramic monolith.

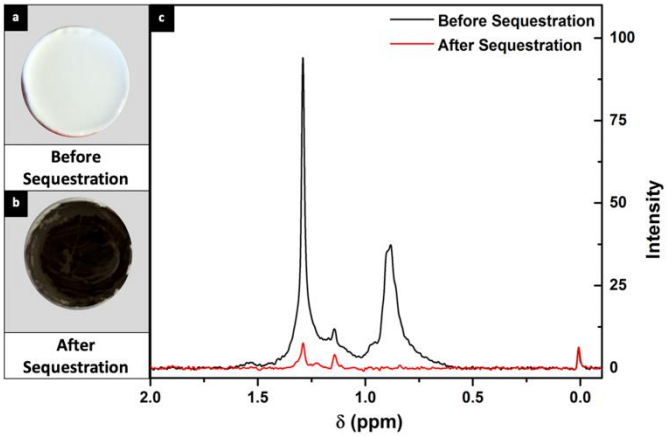

Fig 4 a) Top view of MHO ceramic before sequestration, b) Top view of MHO ceramic after sequestration of crude oil-in-water emulsion in neutral pH, c) ^{1}H NMR spectrum of crude oil-in-water emulsion before and after sequestration with MHO ceramic.

typical oil spill concentrations.[33–36] In **Figure 3a**, we observe a significant reduction in turbidity after filtration was performed using MHO ceramics. GC-MS was used to experimentally support the observation that the oil-in-water emulsion became less turbid after filtration. The resulting chromatogram **in Figure 3b** shows that prior to filtration there are numerous peaks at different relative intensities corresponding to various components of the crude oil mainly hydrocarbon chains ranging from C11 to C34. For comparison purposes, filtration with a cellulose-based filter paper and a melamine sponge was performed. As shown in **Figure 3b**, all crude oil characteristic peaks were still present after filtrations with each of the materials at similar retention times but with lower intensities. Remarkably, filtrations using MHO ceramic and the commercial wine filter (pore size 1 μm) yielded completely clear liquids and there were no crude oil characteristic peaks which is indicative of near 100% removal of crude oil. Similar results were observed with MHO ceramic and the commercial wine filter at extreme acidic (pH 1) and basic conditions (pH 13) as shown in **Fig S2** and **Fig S3** respectively. To confirm and quantify this near 100% removal of crude oil, the liquid samples were analysed using ^{1}H NMR spectroscopy.

Figure 4a shows the MHO ceramic before sequestration and **Figure 4b** shows the MHO ceramic after sequestration in neutral pH. **Figure 4c** illustrates the ^{1}H NMR spectra detailing crude oil-in-water emulsion before and after filtration. From **Figure 4c** we observe crude oil signals at 0.9 ppm for alkyl terminal methyl groups (R-CH_3) and 1.3 ppm for alkyl methylene groups (R-CH_2-R) in the crude oil-in-water emulsion before filtration.[37,38] After filtration the peak at 0.9 ppm was no longer present and the signal at 1.3 ppm showed diminished relative intensity. This pronounced decrease in relative intensity was determined to correspond to a 99.9% removal of crude oil from water. The peak at 1.15 ppm is due to the solvent mixture (**Fig S4**). Other ^{1}H NMR signals are TMS that appears at 0 ppm and the area remains the same before and after filtration indicating the precision of the calibration. Similar results were observed in extreme acidic (pH 1) and basic (pH 13) conditions using MHO ceramic and the commercial wine filter (as shown in **Fig S5-S7**). Altering the pH can influence ionization of the contaminant molecule which can effect sequestration capacities.[39] However, changing the pH did not have an effect on crude oil sequestration because of the inert nature of crude oil. Crude oil is mainly composed of long hydrocarbon chains with strong C-C and C-H bonds which are stable in extreme pH. Furthermore, these alkanes do not have any hydrophilic or ionizable groups that can be influenced by change in pH.[40] **Table S1** offers a comparison between MHO ceramic and the cellulose wine filter, another ceramic membrane made of TiO_2,[41] carbon nanotube based material,[42] magnesium hydroxide formed *in-situ*,[43] and a polyurethane sponge modified with hydrophobic silica nanoparticles.[16] MHO and the cellulose wine filter have similar removal percentages, although the MHO ceramic is a more promising option as it can be readily regenerated by calcination.

3.3 Regeneration of MHO Ceramic Monolith

The reusability of materials used to clean oil spills is imperative, as it decreases the amount of waste produced during the clean-up and enhances the effectiveness of the material deployed. Other materials such as silica-based ceramics[44] and twisted carbon fiber aerogels[45] have been successfully regenerated to remove organic contaminants from water by calcination. This is relatively safer than using harsh and toxic chemicals to clean the material, as it does not produce excess toxic liquid waste. To compare the thermal stability and regeneration of MHO ceramic with the commercial wine filter we performed TGA experiments after filtration with the crude oil-in-water emulsion. Both the MHO ceramic and the wine filter were exposed to 800°C under high purity argon flow. The results of the TGA are shown in **Fig S8a** for MHO ceramic and **Fig S8b** for the wine filter. The mass loss observed from heating the bare MHO ceramic before sequestration is 0.3% which is due to the evaporation of water from the hydrophilic surface. After sequestration of the crude oil-in-water emulsion we see a mass loss of 1.3 % which corresponds to the crude oil and some water

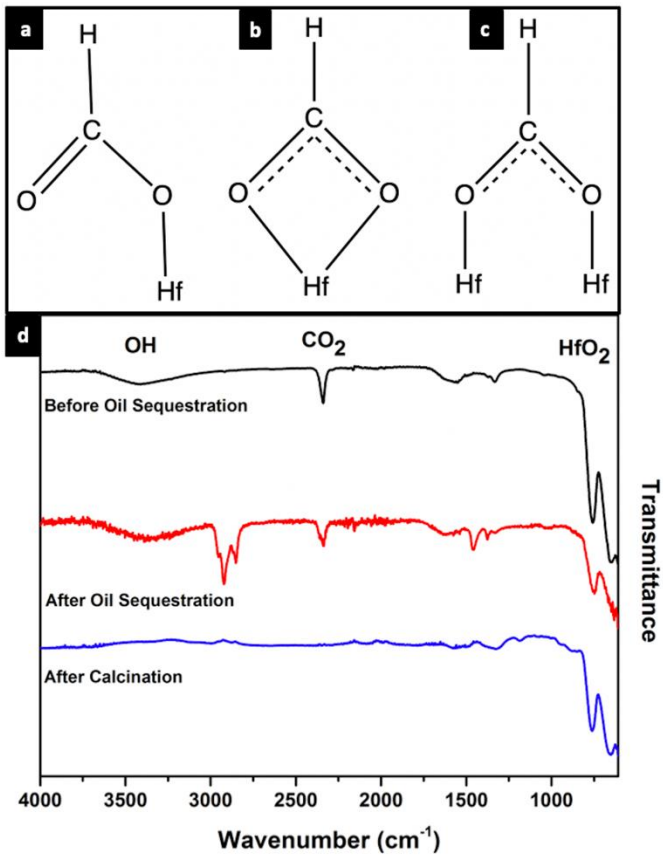

Fig 5 a) Monodentate coordination of one oxygen atom to one hafnium ion, b) Bidentate chelating of two oxygen atoms to one hafnium ion, c) Bidentate bridging of two oxygen atoms to two hafnium ions, and d) ATR-FTIR spectrum of MHO ceramic before sequestration, after sequestration in neutral pH, and after calcination.

evaporating from the MHO ceramic. In contrast, the mass loss observed from heating the bare wine filter before sequestration is 46.1% which is due to the degradation of the wine filter. After sequestration of the crude oil-in-water emulsion a mass loss of 48.7% is the result of the wine filter burning as it is not stable under high temperatures. After these experiments, we observed that the MHO ceramic showed its characteristic white color, and the wine filter had turned entirely black. To ensure that MHO ceramic could be regenerated after each filtration FTIR was done on the surface after calcination to confirm that oil was no longer present as shown in **Figure 5d**.

The FTIR peaks present between 400-800 cm^{-1} represent the monoclinic hafnium oxide peaks of Hf-O and Hf-O_2. During the initial hydrolysis step of the sol-gel synthesis, N-methyl formamide undergoes hydrolysis in water to produce formic acid (HCOOH). As a result, the formato ligands from formic acid coordinate to the Hf ions. The low intensity peaks in the range of 1200-1600 cm^{-1} observed in the MHO ceramic before oil sequestration correspond to symmetric and antisymmetric formato (COO^-) ligand vibrations on the surface of MHO. The three possible types of bonding of the formato ligand to the hafnium ions on the surface of MHO are shown in **Fig 5a-c**. **Fig 5a** illustrates a monodentate coordination of one oxygen atom from the formato ligand to one hafnium ion. **Figure 5b** is a chelating of two oxygen atoms to one hafnium ion. **Fig 5c** is an example of a bridging of two oxygen atoms to two hafnium ions.[46] The peak at 1300 cm^{-1} corresponds to monodentate coordination of carbonates as shown in in **Fig 5a**. The peak at 1600 cm^{-1} represents bidentate carbonates through either chelating of two oxygen atoms to one hafnium (**Fig 5b**) or bridging of two hafnium with two oxygen atoms (**Fig 5c**). The chelating bidentate and bridging bidentate convert to one another based on the degree of hydration on the surface. The peak at 2390 cm^{-1} is identified as CO_2. CO_2 interacts with the Lewis acid sites on the surface through σ-coordination from one of the lone pairs on oxygen.[47] The spectrum from the sample after filtration has the Hf-O and Hf-O_2 peaks from the monoclinic hafnium oxide. The peaks that are present in the sample after sequestration that are not present after calcination are the peaks at 1350 cm^{-1} and 1450 cm^{-1} which correspond to the C-H deformation vibration and the peaks at 2800 cm^{-1} and 2900 cm^{-1} which correspond to the C-H stretching vibration all in aliphatic hydrocarbon chains.[48] A detailed FTIR spectrum of pure crude oil is depicted in **Fig S9**. The spectrum after calcination does not show any of the sharp peaks that were present in the sample after crude oil sequestration. This further proves that there was no crude oil after calcination and MHO ceramic can be regenerated. Similar results were observed in acidic and basic pH as shown in **Fig S10** and **Fig S11**, respectively.

In this case, we believe that the governing aspect of adsorption during filtration is the adhesion of the hydrophobic crude oil to the hydrophilic MHO ceramic.[49] Since the solution at hand is an oil-in-water emulsion coalescence is necessary for de-emulsification of the mixture. During the coalescence process the smaller oil droplets attach on to the hydrophilic surface of the MHO ceramic followed by agglomeration of larger droplets. The physical force dominating the adhesion of the hydrophobic crude oil to the hydrophilic MHO ceramic is most likely Van der Waals (VdW) forces. VdW forces are weak intermolecular forces resulting from electrostatic interactions in typically non-attracting molecules due to asymmetric electronic distributions. Small electronic dipoles are created which can induce dipoles in complementary surfaces. Larger molecules have a higher propensity of remaining in the adsorbed state and that is due to VdW forces. The longer the chain the more electron clouds that can be distorted and can interact with the surface of MHO. VdW forces are weak physical forces which means that the process is reversible. Since no chemical bonds are formed, regeneration of the MHO ceramic can be achieved by calcination of the material after crude oil sequestration as demonstrated herein.[50]

Conclusions

An environmentally benign, mechanically stable, and renewable MHO ceramic monolith was synthesized through a sol-gel process leading to a crystalline bimodal material with macropores and mesopores. The monolith showed excellent adsorption of crude oil from oil-in-water emulsions in acidic, neutral, and basic pH. The material was regenerated by calcination to remove crude oil form the surface. Regeneration of MHO ceramic surface after calcination demonstrates an

underexplored family class of materials that are robust under extreme conditions.

Future work for this project will involve development of Langmuir and Freundlich isotherms. The Langmuir adsorption isotherm is used to describe adsorption of a monolayer of oil on a homogeneous surface of an adsorbent. Meanwhile, the Freundlich isotherm model is used to describe multilayer adsorption of oil on a heterogeneous adsorbent surface. When it comes to a complex mixture such as that of crude oil, using either the Langmuir or Freundlich isotherms is challenging.[51] This is due to the fact that not all components of crude oil obey these isotherms as single solutes, hence in order to calculate the constants for each isotherm one would need to be able to calculate the adsorption coefficient of each solute prior to the isotherm application.

Conflicts of interest

There are no conflicts to declare.

Acknowledgements

We would like to acknowledge the University of California, Davis for start-up funding for this project, as well as support from the Cottrell Scholar program supported by the Research Corporation for Science Advancement (RCSA Grant ID#26780). We also acknowledge funding support from the NSF through UC Davis ChemEnergy REU program, grant #1560479. We also acknowledge support from the McNair Scholars program.

References

1 L. Pendleton, A. Comte, C. Langdon, J. A. Ekstrom, S. R. Cooley, L. Suatoni, M. W. Beck, L. M. Brander, L. Burke, J. E. Cinner, C. Doherty, P. E. T. Edwards, D. Gledhill, L.-Q. Jiang, R. J. van Hooidonk, L. Teh, G. G. Waldbusser and J. Ritter, Coral Reefs and People in a High-CO_2 World: Where Can Science Make a Difference to People?, *PLoS One*, 2016, **11**, e0164699.

2 G. Troisi, S. Barton and S. Bexton, Impacts of oil spills on seabirds: Unsustainable impacts of non-renewable energy, *Int. J. Hydrogen Energy*, 2016, **41**, 16549–16555.

3 M. I. Ramirez, A. P. Arevalo, S. Sotomayor and N. Bailon-Moscoso, Contamination by oil crude extraction – Refinement and their effects on human health, *Environ. Pollut.*, 2017, **231**, 415–425.

4 U. S. C. Guard, *On scene coordinator report : Deepwater Horizon oil spill.*, Library of Congress, 2011.

5 S. Sun, Y. Lu, Y. Liu, M. Wang and C. Hu, Tracking an Oil Tanker Collision and Spilled Oils in the East China Sea Using Multisensor Day and Night Satellite Imagery, *Geophys. Res. Lett.*, 2018, **45**, 3212–3220.

6 P. Venkataraman, J. Tang, E. Frenkel, G. L. McPherson, J. He, S. R. Raghavan, V. Kolesnichenko, A. Bose and V. T. John, Attachment of a Hydrophobically Modified Biopolymer at the Oil–Water Interface in the Treatment of Oil Spills, *ACS Appl. Mater. Interfaces*, 2013, **5**, 3572–3580.

7 V. John, C. Arnosti, J. Field, E. Kujawinski and A. MacCormick, The Role of Dispersants in Oil Spill Remediation: Fundamental Concepts, Rationale for Use, Fate, and Transport Issues, *Oceanography*, 2016, **29**, 108–117.

8 S. Kleindienst, J. H. Paul and S. B. Joye, Using dispersants after oil spills: impacts on the composition and activity of microbial communities, *Nat. Rev. Microbiol.*, 2015, **13**, 388.

9 H. K. White, S. L. Lyons, S. J. Harrison, D. M. Findley, Y. Liu and E. B. Kujawinski, Long-Term Persistence of Dispersants following the Deepwater Horizon Oil Spill, *Environ. Sci. Technol. Lett.*, 2014, **1**, 295–299.

10 B. S. Echols, C. J. Langdon, W. A. Stubblefield, G. M. Rand and P. R. Gardinali, A Comparative Assessment of the Aquatic Toxicity of Corexit 9500 to Marine Organisms, *Arch. Environ. Contam. Toxicol.*, 2019, **77**, 40–50.

11 J. Beirão, L. Baillon, M. A. Litt, V. S. Langlois and C. F. Purchase, Impact of crude oil and the dispersant Corexit™ EC9500A on capelin (Mallotus villosus) embryo development, *Mar. Environ. Res.*, 2019, **147**, 90–100.

12 G. Alaa El-Din, A. A. Amer, G. Malsh and M. Hussein, Study on the use of banana peels for oil spill removal, *Alexandria Eng. J.*, 2018, **57**, 2061–2068.

13 O. Abdelwahab, S. M. Nasr and W. M. Thabet, Palm fibers and modified palm fibers adsorbents for different oils, *Alexandria Eng. J.*, 2017, **56**, 749–755.

14 Z. Wang, J. Saleem, J. P. Barford and G. McKay, Preparation and characterization of modified rice husks by biological delignification and acetylation for oil spill cleanup, *Environ. Technol.*, 2018, **39**, 1–12.

15 M. Khosravi and S. Azizian, Synthesis of a Novel Highly Oleophilic and Highly Hydrophobic Sponge for Rapid Oil Spill Cleanup, *ACS Appl. Mater. Interfaces*, 2015, **7**, 25326–25333.

16 A. Atta, M. Abdullah, H. Al-Lohedan and N. Mohamed, Novel Superhydrophobic Sand and Polyurethane Sponge Coated with Silica/Modified Asphaltene Nanoparticles for Rapid Oil Spill Cleanup, *Nanomaterials*, 2019, **9**, 187.

17 Z.-R. Jiang, J. Ge, Y.-X. Zhou, Z. U. Wang, D. Chen, S.-H. Yu and H.-L. Jiang, Coating sponge with a hydrophobic porous coordination polymer containing a low-energy CF_3-decorated surface for continuous pumping recovery of an oil spill from water, *NPG Asia Mater.*, 2016, **8**, e253–e253.

18 E. Barry, A. U. Mane, J. A. Libera, J. W. Elam and S. B. Darling, Advanced oil sorbents using sequential infiltration synthesis, *J. Mater. Chem. A*, 2017, **5**, 2929–2935.

19 S. T. Nguyen, J. Feng, N. T. Le, N. Hoang, V. B. C. Tan and H. M. Dong, Cellulose Aerogel from Paper Waste for Crude Oil Spill Cleaning, *Ind. Eng. Chem. Res.*, 2013, **52**, 18386–18391.

20 H.-P. Cong, X.-C. Ren, P. Wang and S.-H. Yu, Macroscopic Multifunctional Graphene-Based Hydrogels and Aerogels by a Metal Ion Induced Self-Assembly Process, *ACS Nano*, 2012, **6**, 2693–2703.

21 P. Gao, Z. Liu, D. D. Sun and W. J. Ng, The efficient separation of surfactant-stabilized oil–water emulsions

with a flexible and superhydrophilic graphene–TiO 2 composite membrane, *J. Mater. Chem. A*, 2014, **2**, 14082–14088.

22 L. Zhang, Y. Zhong, D. Cha and P. Wang, A self-cleaning underwater superoleophobic mesh for oil-water separation., *Sci. Rep.*, 2013, **3**, 2326.

23 J. Song, S. Huang, Y. Lu, X. Bu, J. E. Mates, A. Ghosh, R. Ganguly, C. J. Carmalt, I. P. Parkin, W. Xu and C. M. Megaridis, Self-Driven One-Step Oil Removal from Oil Spill on Water via Selective-Wettability Steel Mesh, *ACS Appl. Mater. Interfaces*, 2014, **6**, 19858–19865.

24 X. Zhou, F. Wang, Y. Ji, W. Chen and J. Wei, Fabrication of Hydrophilic and Hydrophobic Sites on Polypropylene Nonwoven for Oil Spill Cleanup: Two Dilemmas Affecting Oil Sorption, *Environ. Sci. Technol.*, 2016, **50**, 3860–3865.

25 S. Govender and H. B. Friedrich, Monoliths : A Review of the Basics , Preparation Methods and Their Relevance to Oxidation, *Catalysts,* 2017, **7**, 1–29 .

26 A. Cybulski and J. A. Moulijn, Monoliths in Heterogeneous Catalysis, *Catal. Rev.*, 1994, **36**, 179–270.

27 V. Tomašić and F. Jović, State-of-the-art in the monolithic catalysts/reactors, *Appl. Catal. A Gen.*, 2006, **311**, 112–121.

28 D. Lu, T. Zhang and J. Ma, Ceramic Membrane Fouling during Ultrafiltration of Oil/Water Emulsions: Roles Played by Stabilization Surfactants of Oil Droplets, *Environ. Sci. Technol.*, 2015, **49**, 4235–4244.

29 J. Nawrocki, M. Rigney, A. McCormick and P. Carr, Chemistry of zirconia and its use in chromatography, *J. Chromatogr. A*, 1993, **657**, 229–282.

30 I. M. Ferrer-Lassala, Ph.D. thesis, SUNY Buffalo, 2013.

31 S. Palchoudhury and J. R. Lead, A Facile and Cost-Effective Method for Separation of Oil − Water Mixtures Using Polymer-Coated Iron Oxide Nanoparticles, *Environ. Sci. Technol.*, 2014, **48**, 14558–14563.

32 W. J. Robson, P. A. Sutton, P. Mccormack, N. P. Chilcott and S. J. Rowland, Class Type Separation of the Polar and Apolar Components of Petroleum, *Anal. Chem.*, 2017, **89** 2919–2927.

33 S. Palchoudhury and J. R. Lead, A Facile and Cost-Effective Method for Separation of Oil–Water Mixtures Using Polymer-Coated Iron Oxide Nanoparticles, *Environ. Sci. Technol.*, 2014, **48**, 14558–14563.

34 R. Almeda, Z. Wambaugh, C. Chai, Z. Wang, Z. Liu and E. J. Buskey, Effects of crude oil exposure on bioaccumulation of polycyclic aromatic hydrocarbons and survival of adult and larval stages of gelatinous zooplankton, *PLoS One*, 2013, **8**, e74476–e74476.

35 R. H. Carmichael, A. L. Jones, H. K. Patterson, W. C. Walton, A. Pérez-Huerta, E. B. Overton, M. Dailey and K. L. Willett, Assimilation of Oil-Derived Elements by Oysters Due to the Deepwater Horizon Oil Spill, *Environ. Sci. Technol.*, 2012, **46**, 12787–12795.

36 J. Vilcáez, L. Li and S. S. Hubbard, A new model for the biodegradation kinetics of oil droplets: application to the Deepwater Horizon oil spill in the Gulf of Mexico, *Geochem. Trans.*, 2013, **14**, 1–14 .

37 L. Díaz-Ballote, N. U. García-Cruz, E. Hernández-Nuñez, A. Castillo-Atoche, G. González-García and G. Rodriguez-Gattorno, *Quim. Nova*, 2018, **41**, 969–973.

38 I. Rakhmatullin, S. Efimov, M. Varfolomeev and V. Klochkov, High-resolution NMR study of light and heavy crude oils: “structure-property” analysis, *IOP Conf. Ser. Earth Environ. Sci.*, 2018, **155**, 1–7.

39 R. C. Pereira, P. R. Anizelli, E. Di Mauro, D. F. Valezi, A. C. S. da Costa, C. T. B. V. Zaia and D. A. M. Zaia, The effect of pH and ionic strength on the adsorption of glyphosate onto ferrihydrite, *Geochem. Trans.*, 2019, **20**, 1–14.

40 B. Simonovic, D. Arandjelovic, M. Jovanovic, B. Kovacevic, L. Pezo and A. Jovanovic, Removal of mineral oil and wastewater pollutants using hard coal, *Chem. Ind. Chem. Eng. Q.*, 2009, **15**, 57–62.

41 K. Suresh and G. Pugazhenthi, Cross flow microfiltration of oil-water emulsions using clay based ceramic membrane support and TiO_2 composite membrane, *Egypt. J. Pet.*, 2017, **26**, 679–694.

42 T. H. Ibrahim, M. A. Sabri and M. I. Khamis, Application of multiwalled carbon nanotubes and its magnetite derivative for emulsified oil removal from produced water, *Environ. Technol.*, 2019, **40**, 3337–3350.

43 W. Dong, D. Sun, Y. Li and T. Wu, Rapid removal and recovery of emulsified oil from ASP produced water using in situ formed magnesium hydroxide, *Environ. Sci. Water Res. Technol.*, 2018, **4**, 539–548.

44 G. M. K. Tolba, A. M. Bastaweesy, E. A. Ashour, W. Abdelmoez, K. A. Khalil and N. A. M. Barakat, Effective and highly recyclable ceramic membrane based on amorphous nanosilica for dye removal from the aqueous solutions, *Arab. J. Chem.*, 2016, **9**, 287–296.

45 H. Bi, Z. Yin, X. Cao, X. Xie, C. Tan, X. Huang, B. Chen, F. Chen, Q. Yang, X. Bu, X. Lu, L. Sun and H. Zhang, Carbon Fiber Aerogel Made from Raw Cotton: A Novel, Efficient and Recyclable Sorbent for Oils and Organic Solvents, *Adv. Mater.*, 2013, **25**, 5916–5921.

46 T. Nishide, T. Meguro, S. Suzuki and T. Yabe, Ultraviolet Irradiation Hardening of Hafnia Films Prepared by Sol-Gel Processes, *J. Ceram. Soc. Japan*, 2005, **113**, 77–81.

47 C. Morterra, G. Cerrato, V. Bolis and B. Fubini, A characterization of the surface acidity of HfO_2 by FTIR spectroscopy of adsorbed species, electron microscopy and adsorption microcalorimetry, *Spectrochim. Acta Part A Mol. Spectrosc.*, 1993, **49**, 1269–1288.

48 A. Samanta, K. Ojha and A. Mandal, Interactions between Acidic Crude Oil and Alkali and Their Effects on Enhanced Oil Recovery, *Energy & Fuels*, 2011, **25**, 1642–1649.

49 S. Bansal, V. von Arnim, T. Stegmaier and H. Planck, Effect of fibrous filter properties on the oil-in-water-emulsion separation and filtration performance, *J. Hazard. Mater.*, 2011, **190**, 45–50.

50 S. De Gisi, G. Lofrano, M. Grassi and M. Notarnicola, Characteristics and adsorption capacities of low-cost sorbents for wastewater treatment: A review, *Sustain. Mater. Technol.*, 2016, **9**, 10–40.

51 R. Wahi, L. A. Chuah, T. S. Y. Choong, Z. Ngaini and M. M. Nourouzi, Oil removal from aqueous state by natural

fibrous sorbent: An overview, *Sep. Purif. Technol.*, 2013, **113**, 51–63.

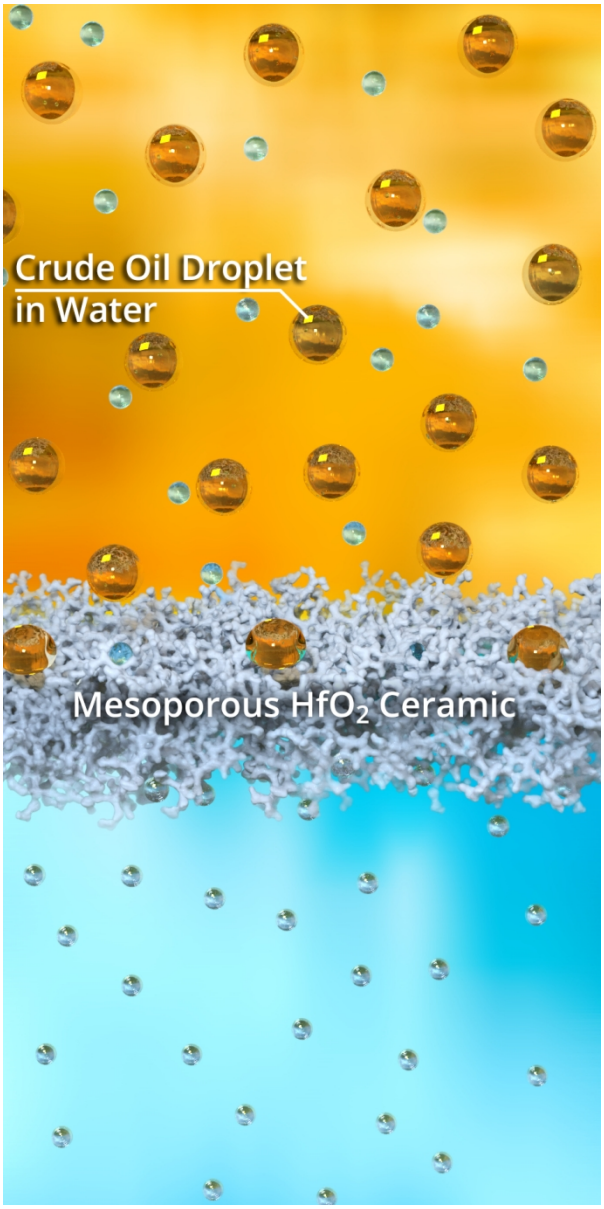

333x666mm (72 x 72 DPI)